Mamba - A Waterproof Snake Robot with Tactile Sensing

Pål Liljebäck, Øyvind Stavdahl, Kristin Y. Pettersen, and Jan Tommy Gravdahl

***Abstract*— This paper presents the snake robot *Mamba*, which is a modular, reconfigurable, and waterproof experimental platform developed to support the ongoing research on snake robot locomotion, including underwater locomotion. A novel contribution of the snake robot is its ability to measure environment contact forces acting along its body, which is achieved by isolating the actuator inside each joint module with a custom-designed force/torque sensor. The paper describes the design of this sensor and presents experimental results which illustrate its performance.**

I. Introduction

Snake robots are robotic mechanisms designed to move like biological snakes [1]. The advantage of such mechanisms is their long and flexible body, which gives them the potential to move and operate in challenging environments where human presence is undesirable or impossible.

The authors' research on snake robot locomotion is based on the hypothesis that intelligent and efficient locomotion in unknown and cluttered environments requires that the snake robot can *sense* its environment and *adapt* its body shape and movements accordingly [2]. Environment sensing for snake robots has received limited attention in previous literature. The world's first snake robot, which was developed by Hirose already in 1972 [1], was equipped with discrete contact switches along its body. A similar approach for environment sensing is employed by the wheel-less snake robot presented in [3]. A snake robot with active wheels, where each wheel axis is equipped with a 3-axial force sensor, is presented in [4], while a snake robot based on active wheels combined with joint torque sensors is presented in [5]. Wheeled snake robots with force sensors based on strain gauges are presented in [6], [7], while the design of a snake-like robot with a soft body integrated with compliant piezo-resistive sensors is presented in [8]. A snake robot covered by smooth shells mounted on top of force sensing resistors is presented in [2], and a similar approach is also proposed in [9].

In addition to environment sensing capabilities, practical applications of snake robots will generally require a waterproof and dustproof design. However, this combination is challenging since the inclusion of an environment sensing system often comes at the expense of electronics which is exposed to the environment. Only a few previous snake robots combine a form of environment sensing with a waterproof design, such as the snake robot with active wheels and joint torque sensors presented in [5].

Fig. 1. The snake robot *Mamba*.

In this paper, we present *Mamba*, which is a modular, reconfigurable, and waterproof snake robot. The main contribution of the robot compared to previous snake robot designs is its novel approach for measuring contact forces and torques acting along its body. This sensor capability is achieved by strain gauge based force/torque sensors installed in each joint module of the robot. Moreover, Mamba combines this sensor capability with a waterproof robot design, which facilitates applications of the robot in outdoor and underwater environments. The paper describes the design of the force/torque sensor and presents experimental results which illustrate its performance.

This paper extends preliminary results in [10], where the authors presented an early version of the force/torque sensor and the joint module of Mamba. This paper presents the design of the complete snake robot, including the final version of the force/torque sensor, which is more sensitive and more accurate than the sensor proposed in [10].

The paper is organized as follows. Section II presents an overview of the robot, while its specific modules are presented in Sections III, IV, and V. Section VI presents the tactile sensor system of the robot, while an experimental investigation of its performance is presented in Section VII. Finally, Section VIII presents concluding remarks.

II. Overview of the Robot

The snake robot *Mamba* is a mechanically robust and easily reconfigurable experimental platform developed to support the ongoing research on snake robot locomotion.

Affiliation of Pål Liljebäck is shared between the Dept. of Engineering Cybernetics at the Norwegian University of Science and Technology (NTNU), 7491 Trondheim, Norway, and SINTEF ICT, Dept. of Applied Cybernetics, 7465 Trondheim, Norway. E-mail: Pal.Liljeback@itk.ntnu.no.

Kristin Y. Pettersen is with the Centre for Autonomous Marine Operations and Systems, Dept. of Engineering Cybernetics at NTNU, 7491 Trondheim, Norway. E-mail: Kristin.Y.Pettersen@itk.ntnu.no.

Øyvind Stavdahl and Jan Tommy Gravdahl are with the Dept. of Engineering Cybernetics at NTNU, 7491 Trondheim, Norway. E-mail: {Oyvind.Stavdahl, Tommy.Gravdahl}@itk.ntnu.no.

This work was partly supported by the Research Council of Norway through project no. 205622 and its Centres of Excellence funding scheme project no. 223254.

TABLE I
PARAMETERS OF THE JOINT MODULE.

Parameter	Value
Weight	310 g
Width/height	70 mm
Length between joint axes	89 mm
Degrees of freedom	1
Max joint travel	$\pm 90^\circ$
Max continuous joint torque	2.3 Nm
Max joint speed (no load)	$429^\circ/\text{sec}$

Environment sensing for snake robots has received limited attention in previous literature and truly adaptive locomotion in cluttered environments has, to the authors' best knowledge, not yet been demonstrated. Mamba was developed to target these limitations in previous literature. The main features of the robot are as follows:

1) **Modular** - The robot has a modular design with a common mechanical and electrical interface between the modules.
2) **Waterproof** - All modules of the robot are waterproof at water depths down to at least 2 m.
3) **Tactile sensing** - The robot can measure forces and torques acting along its body.

The types of modules that we have developed for Mamba so far are shown in Fig. 2 and include (a) head modules, (b) joint modules, (c) joint modules with passive wheels, propulsion modules with motorized (d) wheels, (e) legs, and (f) fins (for swimming), and (g) tail modules. The modules, whose casings have been 3D printed in plastic using selective laser sintering, can be connected with a relative orientation of 0°, 90°, 180°, or 270°. Examples of configurations of the modules are given in Fig. 3. Furthermore, the motion capabilities of a configuration with 12 joint modules is exemplified in Fig. 4, which shows snapshots of the robot during *sidewinding* motion.

In the following sections, we provide a more detailed description of each module along with a detailed description of the tactile sensor system of the robot.

III. THE JOINT MODULE

The joint module of Mamba is shown in Fig. 2(b) and is characterised by the parameters summarised in Table I. A variant of the module is shown in Fig. 2(c), where passive wheels have been mounted to the module to achieve anisotropic ground friction properties for the purpose of efficient locomotion on flat surfaces.

The internal components of the joint are shown in Fig. 5 and are reached through an inspection lid. A Hitec servo motor (HSR-5990TG) is connected directly to the joint shaft and is connected to the module casing via the force/torque sensor presented in Section VI. The sensors inside the joint also include two temperature sensors, a 3-axis accelerometer, and a water leakage detector. The joint is controlled using a microcontroller card (TITechSH2 Tiny Controller from HiBot), which communicates with other modules over a CAN bus. Power supply cables (35 V) run between the modules along with the CAN bus.

Both ends of the joint shaft are sealed using rubber seals and the inspection lid is sealed using an O-ring. Moreover, the entry point of power and CAN bus cables is sealed using a rubber plug. As shown in Fig. 6, the water sealing of the module has been successfully tested at a water depth of 5 meters by placing the module inside a container pressurized by a 5-meter vertical water column.

IV. THE PROPULSION MODULE

The propulsion module of Mamba, which is shown in Fig. 2(d)-(f) and Fig. 7, was developed to support research on motion patterns which combine the articulated structure of the joints with various means of active propulsion along the body. The module consists of rubber wheels that are run by a single servo motor (Dynamixel AX-18A) through a ladder chain. As shown in Fig. 7, the wheels have mounting holes that allow additional structures related to the propulsion to be mounted. Two such examples are given in Fig. 2(e)-(f), respectively, where legs (for walking) and fins (for swimming) have been mounted to the wheels. Demonstrating the motion capabilities provided by the propulsion module is a topic of ongoing research by the authors.

V. THE HEAD AND THE TAIL MODULE

The head and tail modules of Mamba are shown in Fig. 2(a) and (g), respectively. The tail only contains an anchorage mechanism for the external power supply cable. The head (see Fig. 8) contains a microcontroller card, a wireless camera, an IMU (VectorNav VN-100), a WiFi module (ConnectBlue OWS451) for communication with an external PC, and 4 RGB LEDs used for camera lighting and to display status information to the operator.

VI. THE TACTILE SENSOR SYSTEM

In this section, we present the tactile sensor system of the snake robot. An experimental investigation of the sensor system is presented in Section VII.

A. The Measurement Principle

The idea behind the tactile sensor system of Mamba is to calculate *external* forces based on measurements of *internal* forces that occur at the connection between the links. A major advantage of this approach is that sensors are only required near the joint shafts and that the instrumentation can be well protected *inside* the joint modules.

With the proposed approach, we use measured joint constraint forces to estimate external forces on the robot based on the force balance illustrated in Fig. 9. In particular, Fig. 9 illustrates the forces acting on link $i \in \{1, \ldots, N\}$ of a snake robot with N links of equal mass m interconnected by $N-1$ motorized joints. The joint constraint forces which keep link i connected to link $i-1$ and link $i+1$ are denoted by $-\boldsymbol{h}_{i-1} \in \mathbb{R}^3$ and $\boldsymbol{h}_i \in \mathbb{R}^3$, respectively, and are assumed to be measured. Furthermore, the net contact force from the environment, which includes ground friction and forces from external objects, is denoted by $\boldsymbol{f}_{\text{env},i} \in \mathbb{R}^3$ and is assumed to act on the center of mass (CM) of the link. By denoting the CM position of the link by $\boldsymbol{p}_i \in \mathbb{R}^3$, we can write the force balance of link i as

$$m\ddot{\boldsymbol{p}}_i = \boldsymbol{f}_{\text{env},i} + \boldsymbol{h}_i - \boldsymbol{h}_{i-1} \tag{1}$$

Consequently, we can estimate the net external contact force on link i as

$$\boldsymbol{f}_{\text{env},i} = m\ddot{\boldsymbol{p}}_i - \boldsymbol{h}_i + \boldsymbol{h}_{i-1} \tag{2}$$

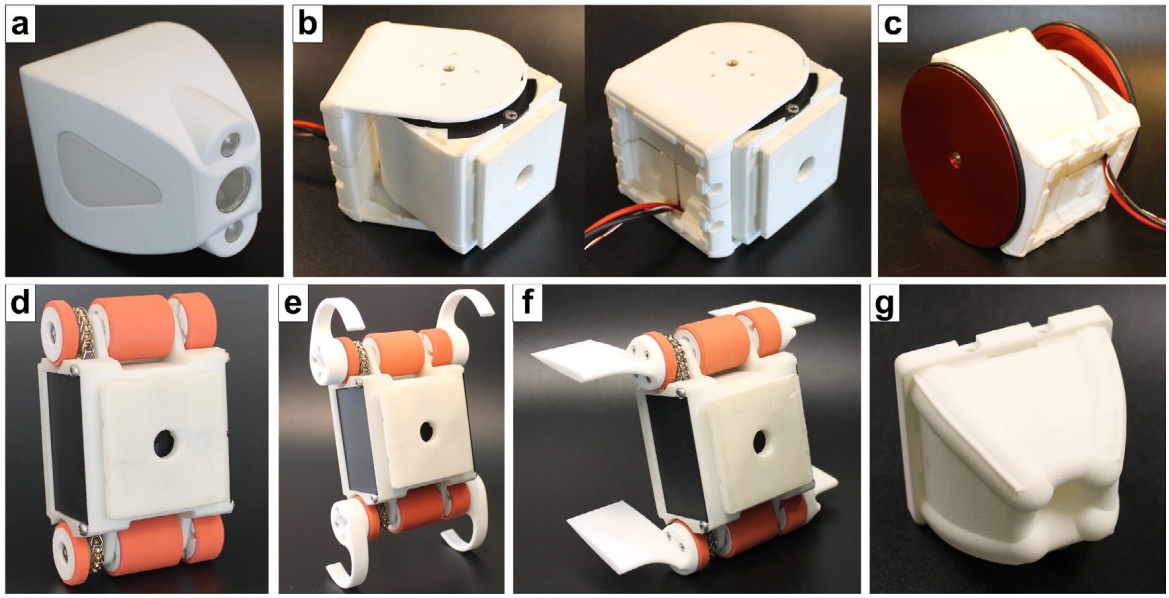

Fig. 2. The modules of the Mamba robot. (a) The head module. (b) The joint module. (c) The joint module with passive wheels. (d) The propulsion module with motorized wheels. (e) The propulsion module with motorized legs. (f) The propulsion module with motorized fins. (g) The tail module.

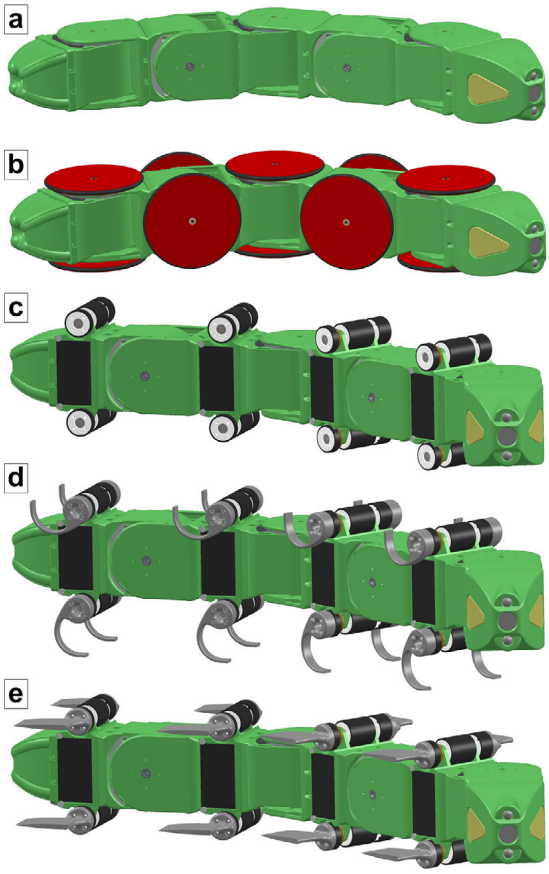

Fig. 3. Examples of Mamba configurations. (a) Configuration with a head, a tail, and several joint modules. (b) Same as (a), but with passive wheels on the joints. (c) Same as (a), but with propulsion modules with motorized wheels mounted between the joints. (d) Same as (c), but with legs mounted on the motorized wheels. (e) Same as (c), but with fins (for swimming) mounted on the motorized wheels.

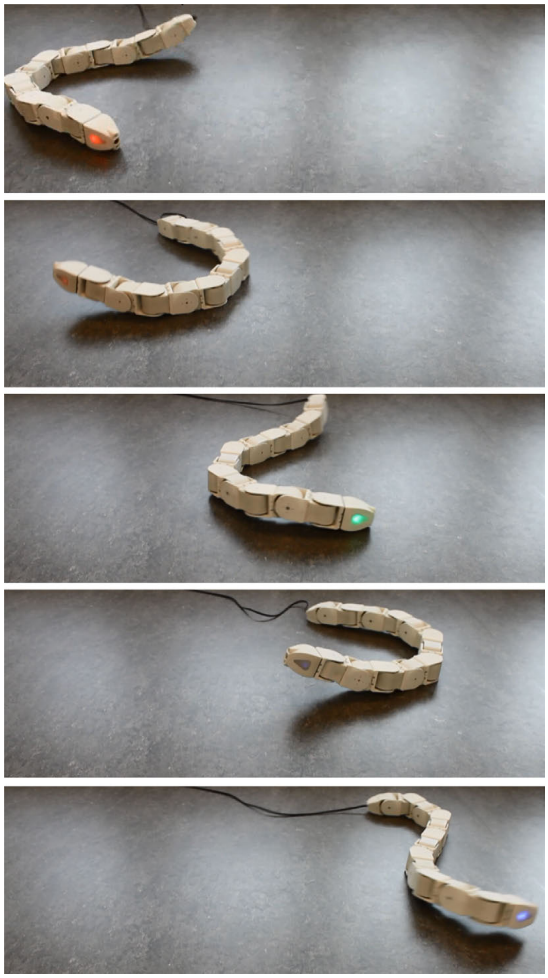

Fig. 4. Mamba *sidewinding* across the floor.

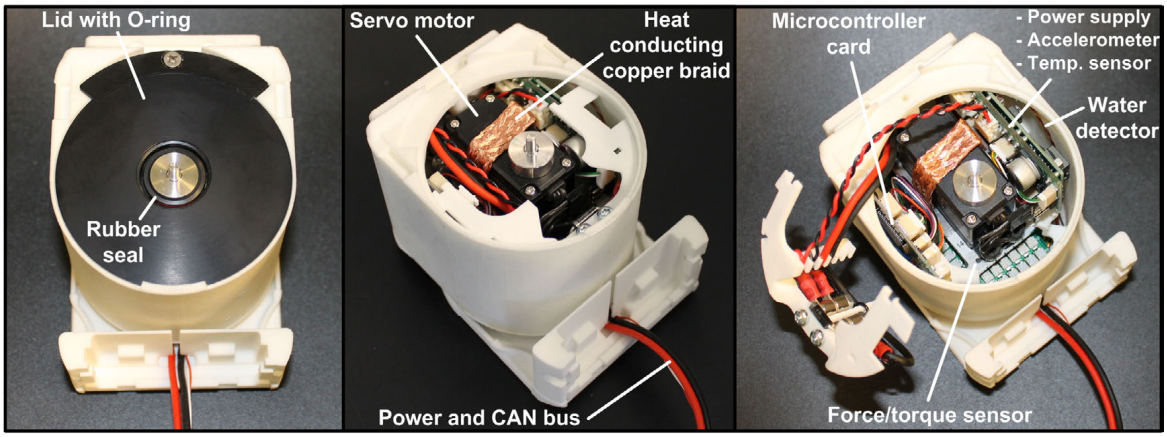

Fig. 5. The components inside the joint module.

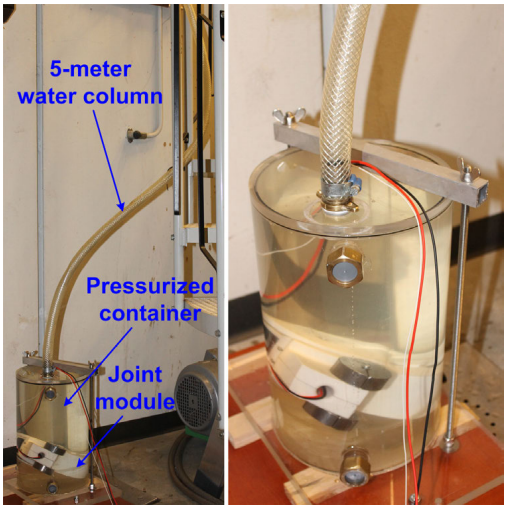

Fig. 6. Experiment which verified that the joint module is waterproof at a water depth of 5 meters.

where the joint constraint forces $\boldsymbol{h}_i$ and $\boldsymbol{h}_{i-1}$ are measured by the force/torque sensor presented in the next subsection, and the acceleration $\ddot{\boldsymbol{p}}_i$ is measured by the accelerometer installed in each joint module of Mamba.

B. The Force/Torque Sensor

The joint constraint forces required to estimate external forces according to (2) are measured by installing a force/torque sensor inside each joint module. The sensor is based on *strain gauges* [11], which were chosen since they are small, accurate, and have a linear characteristic. A strain gauge is used to measure the strain (deformation) of an object, and is basically a resistor whose electrical resistance is proportional to the applied strain. The deformation measured by a strain gauge is very small and usually in the order of 10^{-6} m. In order to measure the corresponding change in resistance, strain gauges are usually connected in a *Wheatstone bridge* arrangement in order to convert the small change in resistance into a voltage signal that can be amplified by an amplifier circuit.

The sensor and its placement in the joint module is illustrated in Fig. 10. As shown in Fig. 10(a), the sensor consists of an aluminium bracket with two wing-like flanges where strain gauges are installed. The joint actuator is mounted directly to this sensor bracket. Moreover, the two wing-like flanges are, as illustrated in Fig. 10(b), secured with screws to the plastic casing of the joint module along with a support bracket, which determines the stiffness (sensitivity) of the sensor. As seen in Fig. 10(c), the wing-like flanges constitute a connection path between the links connected to the joint. Forces and torques acting between the links will therefore cause small deformations of the wing-like flanges that are measured by the strain gauges. The sensor consists of 6 pairs of strain gauges, where each pair is connected in a *half bridge* arrangement [11].

The implemented force/torque sensor is shown in Fig. 11. The aluminium bracket was constructed from an alloy designated 2024-T3, which is particularly well suited for strain gauge measurements. We employed strain gauges from HBM (type K-LY43-0.6/120) with a nominal resistance of 120 Ω and a measurement grid length of 0.6 mm. The strain gauges are wired to a custom-designed amplifier board which provides the sensor output in the form of 6 amplified voltage signals. Potentiometers on the board are used to adjust the gain and the offset of the strain gauge readings.

C. Mapping Strain Gauge Readings to Forces and Torques

We denote the vector of amplified output voltages from the strain gauge amplifier board by $\boldsymbol{V} = [V_1, V_2, V_3, V_4, V_5, V_6]^T \in \mathbb{R}^6$. These voltages are mapped to the measured forces and torques acting on the joint shaft, which we denote by $\boldsymbol{F} = [f_x, f_y, f_z, \tau_x, \tau_y, \tau_z]^T \in \mathbb{R}^6$, and which are defined with respect to the coordinate system shown in Fig. 10(a). In order to estimate the forces and torques in $\boldsymbol{F}$ from the strain gauge readings $\boldsymbol{V}$, we employ a second order mapping model of the form

$$\boldsymbol{F} = \boldsymbol{A}\boldsymbol{V} + \boldsymbol{B}\boldsymbol{V}^2 \tag{3}$$

where $\boldsymbol{A}, \boldsymbol{B} \in \mathbb{R}^{6\times 6}$ are constant matrices and $\boldsymbol{V}^2 = \left[V_1^2, \ldots, V_6^2\right]^T$.

The matrices $\boldsymbol{A}$ and $\boldsymbol{B}$ can be determined through the following calibration procedure for the sensor. We begin by applying $k \geq 6$ known forces/torques to the sensor, denoted by $\boldsymbol{F}_1, \ldots, \boldsymbol{F}_k$, while recording the corresponding output

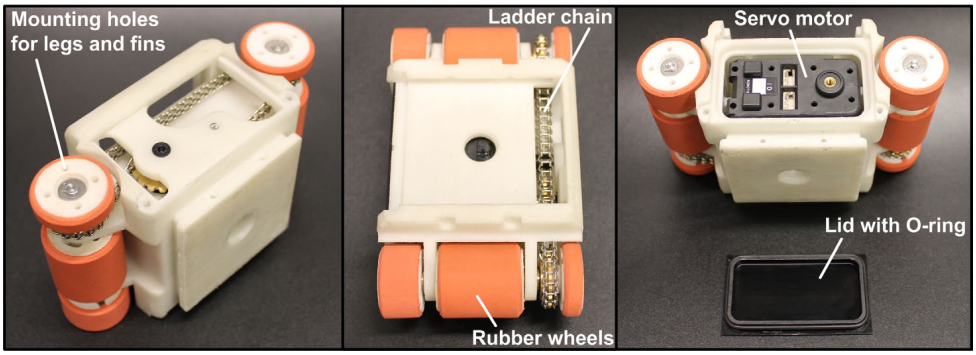

Fig. 7. The components of the propulsion module.

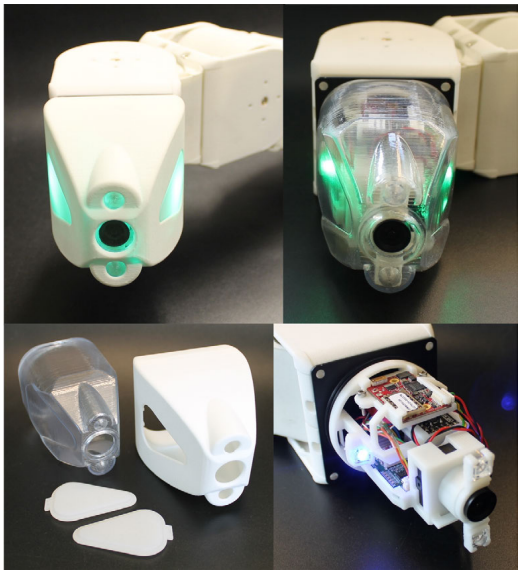

Fig. 8. The head module.

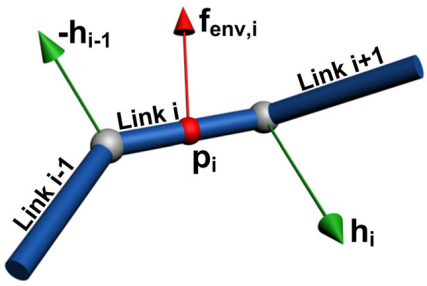

Fig. 9. The joint constraint forces and the environment contact forces acting on the ith link of a snake robot.

voltage vectors $\boldsymbol{V}_1, \ldots, \boldsymbol{V}_k$. The first order mapping matrix $\boldsymbol{A}$ can then be determined by assuming that $\boldsymbol{B} = \boldsymbol{0}$ and using (3) to calculate $\boldsymbol{A}$ as

$$\boldsymbol{A} = [\boldsymbol{F}_1, \ldots, \boldsymbol{F}_k] \, [\boldsymbol{V}_1, \ldots, \boldsymbol{V}_k]^{\dagger} \tag{4}$$

where the inverse of the voltage matrix is calculated according to the Moore-Penrose pseudo inverse. Now that $\boldsymbol{A}$ is defined, it follows from (3) that

$$\boldsymbol{F} - \boldsymbol{A}\boldsymbol{V} = \boldsymbol{B}\boldsymbol{V}^2 \tag{5}$$

which means that $\boldsymbol{B}$ can be calculated as

$$\boldsymbol{B} = [\boldsymbol{F}_1 - \boldsymbol{A}\boldsymbol{V}_1, \ldots, \boldsymbol{F}_k - \boldsymbol{A}\boldsymbol{V}_k] \, [\boldsymbol{V}_1^2, \ldots, \boldsymbol{V}_k^2]^{\dagger} \tag{6}$$

VII. Experimental Investigation of the Force/Torque Sensor

This section presents experimental results which illustrate the performance of the force/torque sensor.

A. Experimental Setup

The experiment was carried out as shown in Fig. 12. In particular, a 3D printed load attachment structure was mounted around the joint. Furthermore, a wire was hooked onto mounting holes on the structure, and steel weights (250 g each) were treaded on the wire according to the desired load on the joint. For each load case, the joint was oriented such that the force from the weights would produce the desired force and torque on the joint.

With reference to the force/torque vector $\boldsymbol{F}$ defined in Section VI-C, we considered the following load cases:

$$\begin{aligned} \boldsymbol{F}^{f_x} &= [f_x^*, 0, 0, 0, 0, 0]^T & \boldsymbol{F}^{\tau_x} &= [0, 0, -f_z^*, \tau_x^*, 0, 0]^T \\ \boldsymbol{F}^{f_y} &= [0, f_y^*, 0, 0, 0, 0]^T & \boldsymbol{F}^{\tau_y} &= [0, 0, -f_z^*, 0, \tau_y^*, 0]^T \\ \boldsymbol{F}^{f_z} &= [0, 0, -f_z^*, 0, 0, 0]^T & \boldsymbol{F}^{\tau_z} &= [0, f_y^*, 0, 0, 0, \tau_z^*]^T \end{aligned} \tag{7}$$

where f_x^*, f_y^*, and f_z^* denote the forces applied by the weights. Furthermore, the torque loads were given by $\tau_x^* = rf_z^*$, $\tau_y^* = rf_z^*$, $\tau_z^* = rf_y^*$, where the torque arm was $r = 59$ mm. The load cases $\boldsymbol{F}^{f_x}$, $\boldsymbol{F}^{f_y}$, and $\boldsymbol{F}^{f_z}$ applied pure forces on the joint, and for each load case we applied 13 different weights. The load cases $\boldsymbol{F}^{\tau_x}$, $\boldsymbol{F}^{\tau_y}$, and $\boldsymbol{F}^{\tau_z}$ applied both forces and torques on the joint, and for each load case we applied 7 different weights. With reference to (4) and (6), this produced a total of $k = 3 \cdot 13 + 3 \cdot 7 = 60$ known force/torque vectors $\boldsymbol{F}_i$ and corresponding voltage readings $\boldsymbol{V}_i$ from the sensor. These vectors were subsequently used to calculate the mapping matrices $\boldsymbol{A}$ and $\boldsymbol{B}$ according to (4) and (6), respectively.

Remark 1: The weight of the load attachment structure applied forces and torques on the joint which varied depending on the orientation of the joint in each load case. To remove the offsets in the strain gauge readings caused by the load attachment structure, the voltage reading *without*

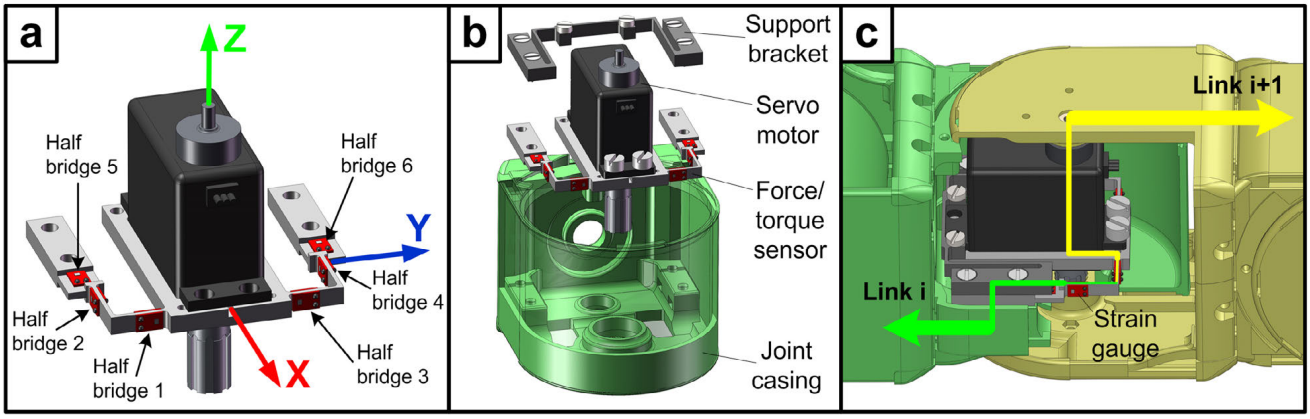

Fig. 10. The design of the force/torque sensor. (a) The sensor coordinate system and the location of the strain gauges. (b) The sensor assembly inside the joint casing. (c) Forces and torques acting between link i and link $i+1$ propagate through the strain gauges.

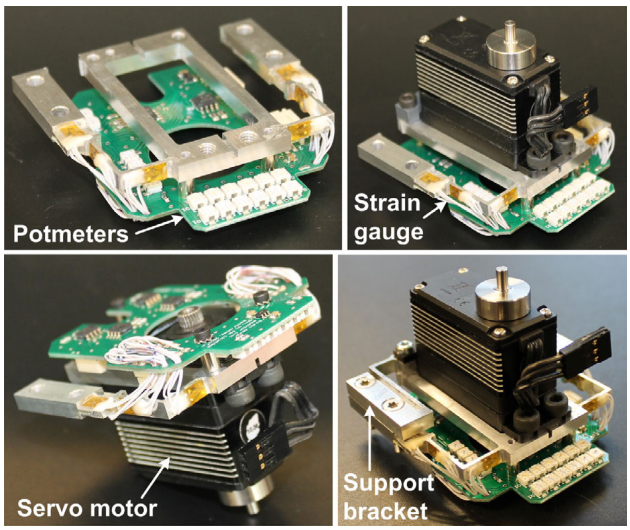

Fig. 11. The force/torque sensor inside each joint module.

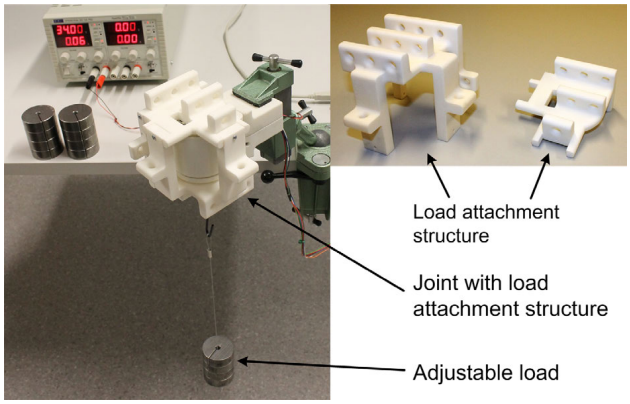

Fig. 12. The experimental setup of the force/torque sensor.

weights applied to the structure was, in each load case, recorded and subtracted from the voltage readings *with* applied weights.

Remark 2: The experiment was carried out *with* the rubber seals at each end of the joint shaft installed. By including these seals during the sensor calibration, the calculated matrices $\boldsymbol{A}$ and $\boldsymbol{B}$ will to some extent compensate for disturbance forces from the seals on the joint shaft.

B. Experimental Results

Using the calculated matrices $\boldsymbol{A}$ and $\boldsymbol{B}$, we mapped each of the $k = 60$ voltage readings to their corresponding force/torque vector according to (3). The estimated forces and torques from the load cases $\boldsymbol{F}^{f_x}$, $\boldsymbol{F}^{f_y}$, and $\boldsymbol{F}^{f_z}$ are plotted in Fig. 13 as a function of the actual applied loads, while the estimated forces and torques from the load cases $\boldsymbol{F}^{\tau_x}$, $\boldsymbol{F}^{\tau_y}$, and $\boldsymbol{F}^{\tau_z}$ are plotted in Fig. 14. The black diagonal line in each plot outlines the ideal correspondance between applied and measured forces/torques. Furthermore, the root-mean-square (RMS) error and the maximum error of the force/torque estimates are presented in Table II.

The plots show a fairly good agreement between the actual and the estimated forces and torques. The RMS error values in Table II suggest that the accuracy of the sensor in average is within ± 1 N for forces and within ± 0.04 Nm for torques. However, the maximum error values in Table II imply that the error in the sensor measurements at times is larger than the RMS error. We believe the inaccuracies of the sensor are primarily caused by disturbance forces on the joint shaft from the rubber seal at each end of the shaft.

The maximum error values in Table II suggest that the force/torque sensors installed in Mamba should not be regarded as high-precision sensors. Nevertheless, the authors conjecture that the sensor accuracy is adequate for demonstrating adaptive locomotion in cluttered environments. In particular, the authors believe that adaptive locomotion may be achieved if the snake robot can detect contact forces and also, to some extent, assess the magnitude of these forces. The experimental results suggest that the sensor system in Mamba is able to meet these requirements. Demonstrating the adaptive motion capabilities of Mamba in cluttered environments is a topic of ongoing investigations by the authors.

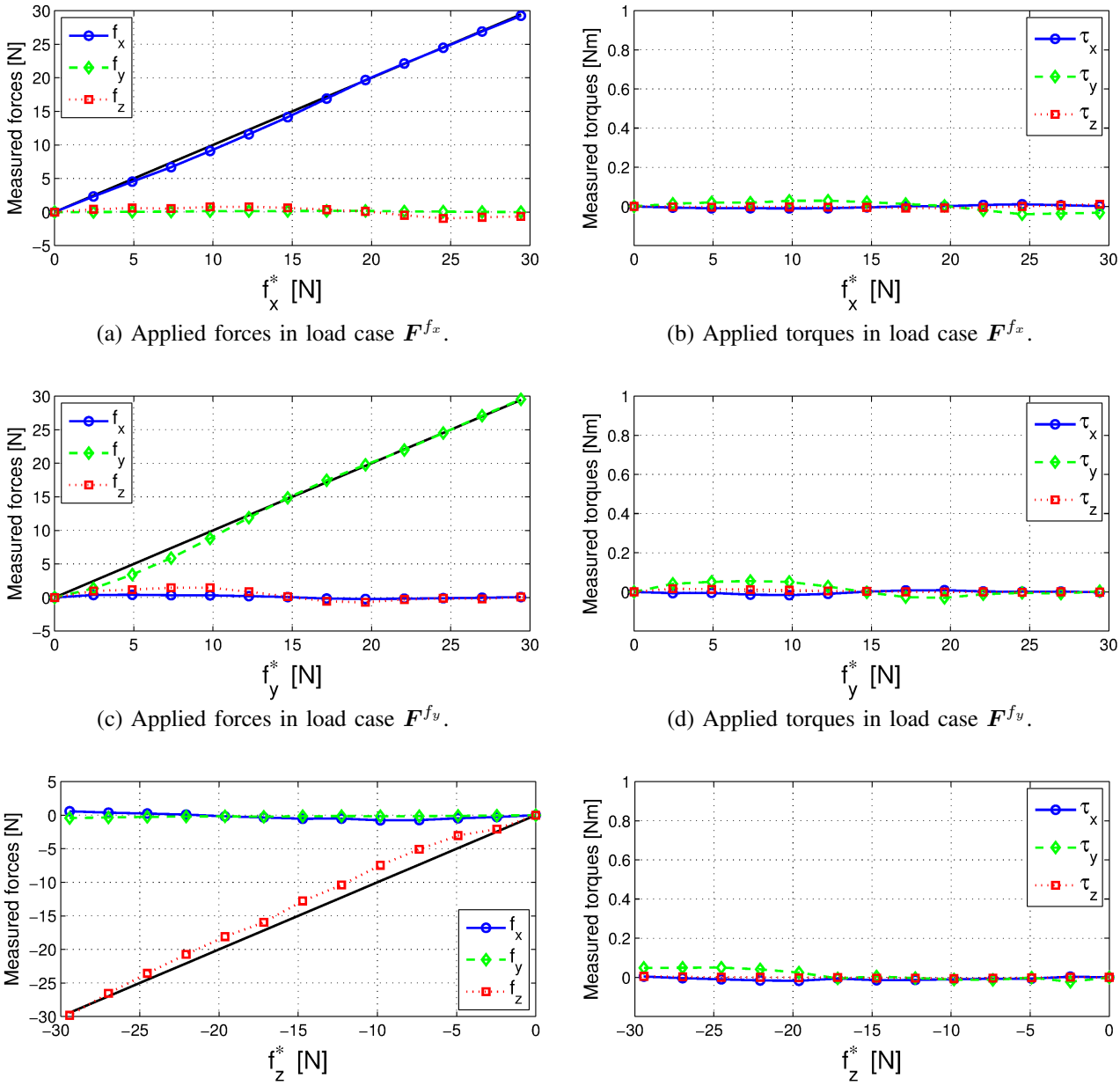

(a) Applied forces in load case $\boldsymbol{F}^{f_x}$.

(b) Applied torques in load case $\boldsymbol{F}^{f_x}$.

(c) Applied forces in load case $\boldsymbol{F}^{f_y}$.

(d) Applied torques in load case $\boldsymbol{F}^{f_y}$.

(e) Applied forces in load case $\boldsymbol{F}^{f_z}$.

(f) Applied torques in load case $\boldsymbol{F}^{f_z}$.

Fig. 13. The measured forces and torques from the load cases where forces, but no torques, were applied to the joint. The black diagonal line in each plot outlines the ideal correspondance between applied and measured forces/torques.

TABLE II
THE ROOT-MEAN-SQUARE (RMS) ERROR AND THE MAX ERROR IN THE ESTIMATED FORCES AND TORQUES.

	f_x	f_y	f_z	τ_x	τ_y	τ_z
RMS error	0.37	0.41	0.96	0.02	0.04	0.01
Max error	0.79	1.49	2.33	0.05	0.16	0.02

VIII. CONCLUSIONS

This paper has presented Mamba, which is a modular and reconfigurable experimental platform developed to support the ongoing research on snake robot locomotion. The robot is waterproof and consists of different types of modules that can be interconnected in many different configurations. In order to measure environment contact forces acting along its body, each joint module of the robot contains a custom-designed sensor (based on strain gauges) that measures the interaction forces and torques between the links. The paper has described the design of the sensor and presented experimental results that illustrate its performance.

REFERENCES

[1] S. Hirose, *Biologically Inspired Robots: Snake-Like Locomotors and Manipulators*. Oxford: Oxford University Press, 1993.

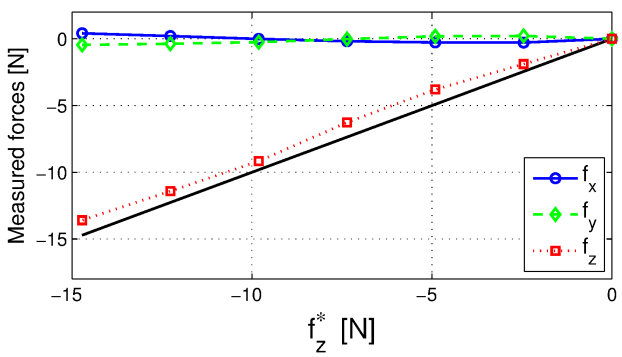

(a) Applied forces in load case $\boldsymbol{F}^{\tau_x}$.

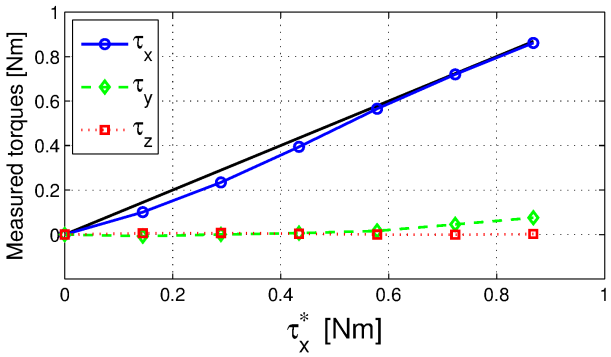

(b) Applied torques in load case $\boldsymbol{F}^{\tau_x}$.

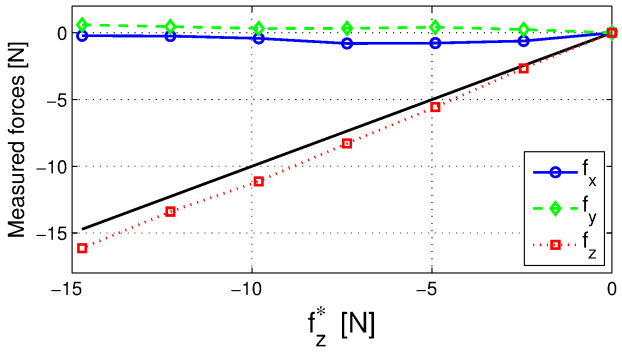

(c) Applied forces in load case $\boldsymbol{F}^{\tau_y}$.

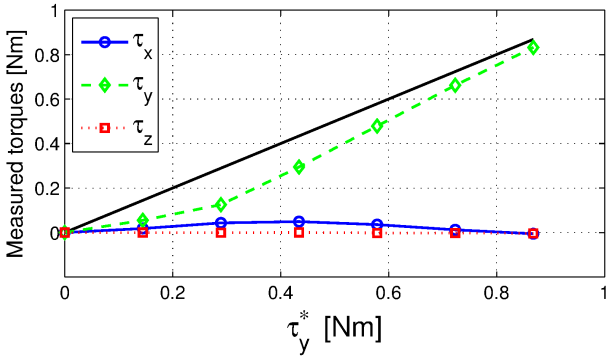

(d) Applied torques in load case $\boldsymbol{F}^{\tau_y}$.

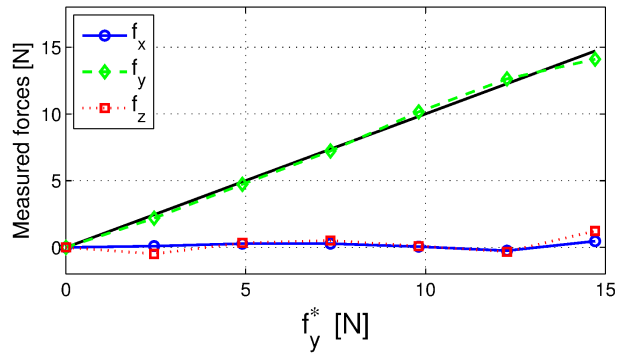

(e) Applied forces in load case $\boldsymbol{F}^{\tau_z}$.

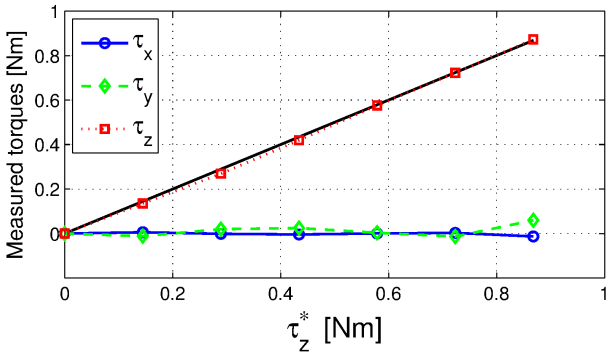

(f) Applied torques in load case $\boldsymbol{F}^{\tau_z}$.

Fig. 14. The measured forces and torques from the load cases where both forces and torques were applied to the joint. The black diagonal line in each plot outlines the ideal correspondance between applied and measured forces/torques.

[2] P. Liljebäck, K. Y. Pettersen, Ø. Stavdahl, and J. T. Gravdahl, *Snake Robots - Modelling, Mechatronics, and Control*, ser. Advances in Industrial Control. Springer, 2013.

[3] Z. Y. Bayraktaroglu, "Snake-like locomotion: Experimentations with a biologically inspired wheel-less snake robot," *Mechanism and Machine Theory*, vol. 44, no. 3, pp. 591–602, 2008.

[4] S. R. Taal, H. Yamada, and S. Hirose, "3 axial force sensor for a semi-autonomous snake robot," in *Proc. IEEE Int. Conf. Robotics and Automation*, 2009, pp. 4057–4062.

[5] S. Takaoka, H. Yamada, and S. Hirose, "Snake-like active wheel robot ACM-R4.1 with joint torque sensor and limiter," in *IEEE/RSJ Int. Conf. Intelligent Robots and Systems*, 2011, pp. 1081–1086.

[6] C. Birkenhofer, M. Hoffmeister, J. Zollner, and R. Dillmann, "Compliant motion of a multi-segmented inspection robot," in *IEEE/RSJ Int. Conf. Intelligent Robots and Systems*, 2005, pp. 2632–2637.

[7] T. L. T. Chen, S. Liu, and J. Yen, "A bio-mimetic snake-like robot: Sensor based gait control," in *Advanced robotics and Its Social Impacts, 2008. ARSO 2008. IEEE Workshop on*, 2008, pp. 1–6.

[8] W. Liu, F. Li, C. Stefanini, D. Chen, and P. Dario, "Biomimetic flexible/compliant sensors for a soft-body lamprey-like robot," *Robotics And Autonomous Systems*, vol. 58, pp. 1138–1148, 2010.

[9] J. Gonzalez-Gomez, J. Gonzalez-Quijano, H. Zhang, and M. Abderrahim, "Toward the sense of touch in snake modular robots for search and rescue operations," in *Proc. ICRA 2010 Workshop "Modular Robots: State of the Art"*, 2010, pp. 63–68.

[10] P. Liljebäck, Ø. Stavdahl, K. Y. Pettersen, and J. T. Gravdahl, "A modular and waterproof snake robot joint mechanism with a novel force/torque sensor," in *Proc. IEEE/RSJ Int. Conf. on Intelligent Robots and Systems*, 2012, pp. 4898–4905.

[11] K. Hoffmann, *An Introduction to Measurements Using Strain Gages*. Hottinger Baldwin Messtechnik GmbH, Darmstadt, 1989.